SST-Vm Model Verification Case

Updated March 2026

1 Equations

The reference for the standard implementation of the Menter SST model is: Menter, F. R., "Two-Equation Eddy-Viscosity Turbulence Models for Engineering Applications," AIAA Journal, Vol. 32, No. 8, August 1994, pp. 1598-1605, `https://doi.org/10.2514/3.12149`. The two-equation model (written in conservation form) is given by the following:

$$\frac{\partial(\rho k)}{\partial t} + \frac{\partial(\rho u_j k)}{\partial x_j} = \mathcal{P} - \beta^* \rho \omega k + \frac{\partial}{\partial x_j}\left[(\mu + \sigma_k \mu_t)\frac{\partial k}{\partial x_j}\right] \tag{1}$$

$$\frac{\partial(\rho \omega)}{\partial t} + \frac{\partial(\rho u_j \omega)}{\partial x_j} = \frac{\gamma}{\nu_t}\mathcal{P} - \beta \rho \omega^2 + \frac{\partial}{\partial x_j}\left[(\mu + \sigma_\omega \mu_t)\frac{\partial \omega}{\partial x_j}\right] + 2(1 - F_1)\frac{\rho \sigma_{\omega 2}}{\omega}\frac{\partial k}{\partial x_j}\frac{\partial \omega}{\partial x_j} \tag{2}$$

Here, ω is the specific rate of dissipation of the turbulence kinetic energy k into internal thermal energy, ρ is the density, u_i is the velocity vector component, x_i is the spatial coordinate, μ_t is the turbulent kinematic viscosity, $\nu_t = \mu_t/\rho$ is the eddy viscosity, μ is the molecular dynamic viscosity, $\mathcal{P}$ is the production term, F_1 is the blending function, and $\sigma_k, \sigma_\omega, \sigma_{\omega 2}, \beta$, and β^* are model constants. This conservative formulation is consistent with formulations used in most original publications, e.g., Wilcox (in Turbulence Modeling for CFD, DCW Industries, Inc., La Canada, CA, 2006, `https://www.amazon.com/Turbulence-Modeling-Third-David-Wilcox/dp/1928729088`) and Menter (in NASA TM 103975, 1992, `https://ntrs.nasa.gov/citations/19930013620`).

Remark 1: There is a consistent non-conservative formulation. Given mass conservation and any smooth scalar function ϕ,

$$\frac{\partial(\rho \phi)}{\partial t} + \frac{\partial(\rho u_j \phi)}{\partial x_j} \equiv \rho \mathcal{D}\phi \tag{3}$$

where

$$\mathcal{D}\phi \equiv \frac{\partial \phi}{\partial t} + u_j \frac{\partial \phi}{\partial x_j} \tag{4}$$

is the Lagrangian (material) derivative. Indeed,

$$\frac{\partial(\rho\phi)}{\partial t} + \frac{\partial(\rho u_j \phi)}{\partial x_j} = \rho\mathcal{D}\phi + \phi\left(\frac{\partial\rho}{\partial t} + \frac{\partial(\rho u_j)}{\partial x_j}\right) \tag{5}$$

and, from mass conservation,

$$\frac{\partial\rho}{\partial t} + \frac{\partial(\rho u_j)}{\partial x_j} = 0 \tag{6}$$

The SST-Vm model is a variant of the Menter SST model. The correction V designates that the production term is based on vorticity magnitude, Ω. The reference for vorticity-based source term is Menter, F. R., "Improved Two-Equation k-omega Turbulence Models for Aerodynamic Flows," NASA TM 103975, October 1992, `https://ntrs.nasa.gov/citations/19930013620`. The little m in Vm indicates that contributions from k are ignored in the Boussinesq approximation for the Reynolds stress tensor, τ_{ij}, in the momentum and energy conservation equations, and the production term is approximated as

$$\mathcal{P} = \min(\mu_t\Omega^2, 20\beta^*\omega k) \tag{7}$$

$$\mu_t = \frac{\rho a_1 k}{\max(a_1\omega, \Omega F_2)}, \quad \Omega = \sqrt{2W_{ij}W_{ij}}, \quad W_{ij} = \frac{1}{2}\left(\frac{\partial u_i}{\partial x_j} - \frac{\partial u_j}{\partial x_i}\right) \tag{8}$$

In the SST model, the production term is limited in the k-equation, but not in the ω-equation. The form of the production limiter (Eq. 7) is suggested in Menter, F. R., "Zonal Two Equation k-omega Turbulence Models for Aerodynamic Flows," AIAA Paper 93-2906, July 1993, `https://doi.org/10.2514/6.1993-2906`. In the ω-equation,

$$\mathcal{P} = \mu_t\Omega^2 \tag{9}$$

Each of the constants in the model is a blend of an inner (1) and outer (2) constant, blended via:

$$\phi = F_1\phi_1 + (1 - F_1)\phi_2 \tag{10}$$

where ϕ_1 represents constant 1 and ϕ_2 represents constant 2. Additional functions are given by:

$$F_1 = \tanh\left(\arg_1^4\right) \tag{11}$$

$$\arg_1 = \min\left[\max\left(\frac{\sqrt{k}}{\beta^*\omega d}, \frac{500\nu}{d^2\omega}\right), \frac{4\rho\sigma_{\omega 2}k}{\mathrm{CD}_{k\omega}d^2}\right] \tag{12}$$

$$\mathrm{CD}_{k\omega} = \max\left(2\rho\sigma_{\omega 2}\frac{1}{\omega}\frac{\partial k}{\partial x_j}\frac{\partial\omega}{\partial x_j}, 10^{-20}\right) \tag{13}$$

$$F_2 = \tanh\left(\arg_2^2\right) \tag{14}$$

$$\arg_2 = \max\left(2\frac{\sqrt{k}}{\beta^*\omega d}, \frac{500\nu}{d^2\omega}\right) \tag{15}$$

Here, d is the distance from the field point to the nearest wall. The constants are:

$$\gamma_1 = \frac{\beta_1}{\beta^*} - \frac{\sigma_{\omega 1}\kappa^2}{\sqrt{\beta^*}} \qquad \gamma_2 = \frac{\beta_2}{\beta^*} - \frac{\sigma_{\omega 2}\kappa^2}{\sqrt{\beta^*}} \tag{16}$$

$$\sigma_{k1} = 0.85 \qquad \sigma_{\omega 1} = 0.5 \qquad \beta_1 = 0.075 \qquad \sigma_{k2} = 1.0 \qquad \sigma_{\omega 2} = 0.856 \tag{17}$$

$$\beta_2 = 0.0828 \qquad \beta^* = 0.09 \qquad \kappa = 0.41 \qquad a_1 = 0.31 \tag{18}$$

2 Geometry

The 3D bump geometry is derived from a 2D bump profile

$$\begin{cases} z = 0.05\left(\sin\left(\frac{\pi x}{0.9} - \frac{\pi}{3}\right)\right)^4, & 0.3 \le x \le 1.2 \\ z = 0, & 0 \le x < 0.3 \quad \text{and} \quad 1.2 < x \le 1.5 \end{cases} \tag{19}$$

Here, z is the vertical direction and x is the streamwise direction. The body reference length is 1.5 units, with the actual bump corresponding to $z > 0$ is at $0.3 < x < 1.2$. The maximum height of the bump is 0.05.

In the 3D setting, the 2D profile is defined along the line $y = 0$. A spanwise (y-directional) variation is added as

$$x = x_0 + 0.3(sin(\pi y))^4, \quad -0.5 \le y \le 0 \tag{20}$$

where x_0 is any given location on the 2D profile, Eq. 19.

3 Boundary Conditions and Flow Parameters

The boundary conditions are defined as follows. Adiabatic no-slip solid-wall boundary conditions are set on the bump surface. The upstream and downstream farfield boundary conditions are set at $x = -25$ and $x = 26.5$, respectively. Constant total pressure and total temperature boundary conditions corresponding to $P_t/P_{ref} = 1.02828, T_t/T_{ref} = 1.008$ are applied at the upstream boundary, and constant pressure boundary conditions corresponding to $P/P_ref = 1$ are applied at the downstream boundary. Symmetry boundary conditions are imposed on the bottom boundary at $z = 0$ between the farfield and the solid wall $-25 < x < 0.3(\sin(\pi y))^4$ and $1.5 + 0.3(\sin(\pi y))^4 < x < 26.5$, on the top boundary at $z = 5.0$, and on the side walls set at $y = 0$ and $y = -0.5$. Figures 1 (a) and (b) show the close-up view of the 2D profile at y = 0 and the layout of the 3D boundary conditions, respectively.

A subsonic ($M_{ref} = 0.2$) compressible turbulent flow is considered. The Reynolds number per unit length is $Re = 3 \times 10^6$. The freestream static temperature is $T_{ref} = 540$ Rankine. The Prandtl number is taken to be constant at $Pr = 0.72$, and the turbulent Prandtl number is taken to be constant at $Pr_t = 0.9$. The molecular viscosity is computed using Sutherland's Law.

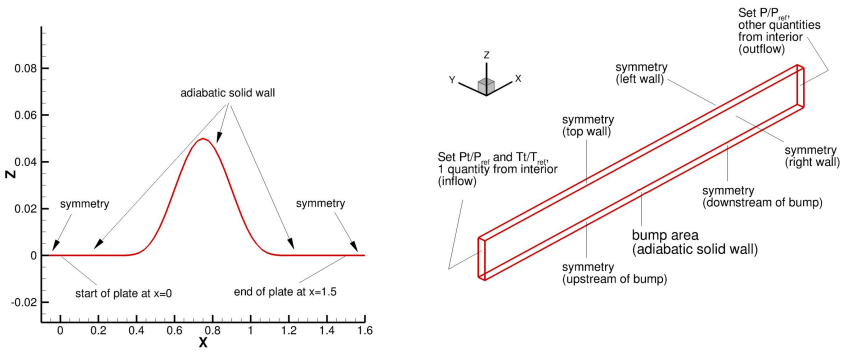

(a) 2D bump profile

(b) 3D bump layout

Figure 1: 3D bump profile and boundary conditions.

$$k_{wall} = 0 \tag{21}$$

$$\omega_{wall} = 10\frac{6\nu}{\beta_1(\Delta d_1)^2} \tag{22}$$

$$k_{farfield} = 9 \times 10^{-9} a_\infty^2 \tag{23}$$

$$\omega_{farfield} = 1 \times 10^{-6}\frac{\rho_\infty a_\infty^2}{\mu_\infty} \tag{24}$$

Here, Δd_1 is the wall distance from the first point off the wall. The farfield values represent the "standard" SST-Vm boundary condition values, chosen to achieve a not-too-low level of freestream turbulent kinetic energy, a not-too-severe rate of freestream turbulence decay, and a reasonable level of freestream turbulent eddy viscosity of $\mu_t/\mu_\infty = 0.009$.

4 Grids

A family of six nested, uniformly-refined 3D hexahedral grids has been generated. Within the family, grids have been generated recursively, starting from the finest grid. Each coarser grid in the family is derived from the preceding finer grid by removing every other grid plane in each dimension. Grids range from the finest $65 \times 1409 \times 641$ grid (Grid 1) to the coarsest $3 \times 45 \times 21$ grid (Grid 6). The grid dimensions represent the numbers of nodes in the spanwise, streamwise, and vertical directions, respectively. Grid 1 has minimum spacing at the wall of 5.0×10^{-7}, giving an approximate average $z^+ = 0.06$ over the bump surface. Even Grid 6 has reasonably fine wall-normal spacing, giving an approximate average $z^+ = 2$ over the bump. The grids are stretched in the wall-normal direction and clustered near the leading and trailing edges. The

spacing in the spanwise direction is uniform. Figures 2 (a) and (b) show the bump surface and a portion of the $9 \times 177 \times 81$ grid. The 2D bump profile and a Fortran code generating the 3D grid family (in the .PLOT3D format) from this profile can be accessed at `https://tmbwg.github.io/turbmodels/bump3d_mod_numerics_val.html`. For convenience, the 3D grids generated in the .ugrid format are also posted at the bottom of the `https://tmbwg.github.io/turbmodels/bump3d_mod_numerics_grids.html` page. Examples of verification output are given for the SA-neg model at `https://tmbwg.github.io/turbmodels/bump3d_mod_numerics_val_sa.html`

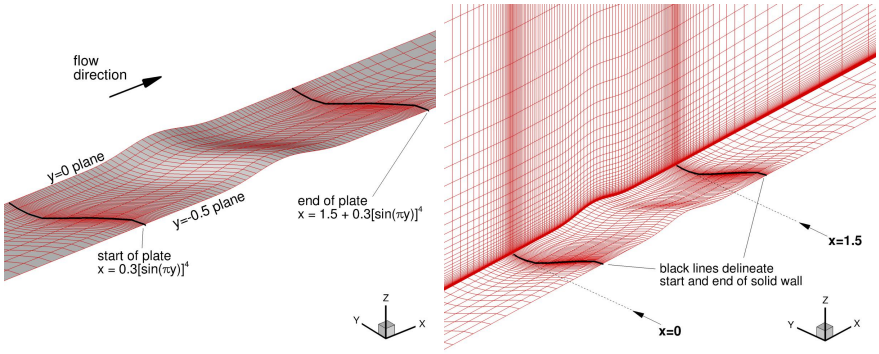

(a) 2D bump profile (b) 3D bump layout

Figure 2: 3D bump geometry.